Supporting Information to the Article: Probing the Structure and Dynamics of Confined Water in AOT Reverse Micelles

Anna Victoria Martinez,[†] Laura Dominguez,[†] Edyta Małolepsza,[†] Adam Moser,[†,‡] Zack Ziegler,[†] and John E. Straub[*,†]

Department of Chemistry, Boston, MA 02215, USA.

E-mail: straub@bu.edu

[*]To whom correspondence should be addressed
[†]Boston University
[‡]Current address: Loras College, Department of Chemistry, Dubuque, IA 52001, USA.

Methods

To construct the RMs, a sphere of water was "cut" from a previously equilibrated water box and minimized with a spherical potential. Random water molecules in the sphere were replaced with sodium counterions (one for each AOT molecule to be added) and re-minimized with the spherical potential. A shell of AOT molecules was built by placing the molecules onto a spherical grid around the water core. Once combined, the water and ions were held fixed, and a spherical potential was placed on the sulfur atoms restraining them to the center. A diameter for the spherical restraint was set depending on the w_0 and composition of the RM, and the system was energy minimized once more. With the spherical potential still in place, the RM was heated to room temperature. Once heated, the potential was removed and 100 ps of dynamics were run to allow the AOT tails to equilibrate before adding the solvent.

The truncated octahedron of isooctane was built using Langevin Dynamics (LD) to generate random isooctane structures. 125 isooctane structures from the LD trajectory were chosen at random and placed on a grid. This cube was minimized, heated and equilibrated before being being cut into a truncated octahedron. The final truncated octahedron was minimized, reheated, and equilibrated. The isooctane and reverse micelle were combined and overlapping isooctane molecules were removed. A constraint was placed on the RM to keep it fixed and to allow the isooctane molecules to adjust around the AOT aliphatic tails. The constraint was removed and the system was energy minimized again at constant temperature and pressure, heated to room temperature, and equilibrated for an additional 100 ps.

Once the construction of the systems was complete, four spherically restrained and four unrestrained RMs were re-minimized, heated to 300 K, and equilibrated at constant temperature and pressure for 500 ps using NAMD.[1] The starting structures for the unrestrained RMs (pre-NAMD re-minimization, etc.) were re-minimized, heated to 300 K and equilibrated for 500 ps using GROMACS and the GROMOS96 53a6 united atom force field.[2]

GROMOS Results

Density

We used GROMACS to compute the solvent accessible surface area with default parameter values[3,4] to calculate the volumes and densities for the GROMOS systems.

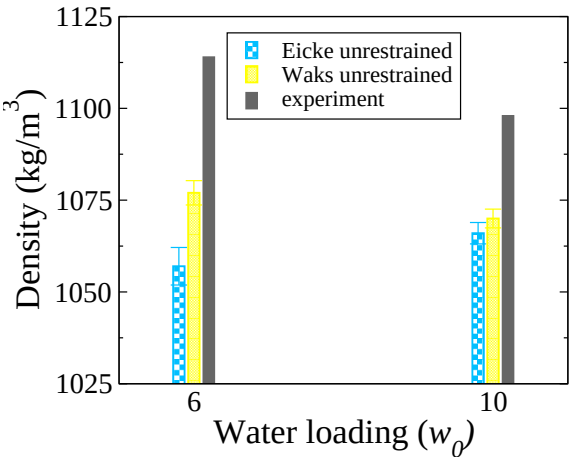

Figure 1: Densities (kg/m^3) for simulated GROMOS RMs. The experimental values are in dark gray. The densities for the unrestrained RMs are in blue and yellow. Calculated values for the GROMOS simulations are within 5% of the reported experimental densities.

Shape Parameters

Table 1: Average values for last 15 ns of simulation time for the moments of inertia I_1, I_2, I_3 (10^6 amu*Å^2), semiaxes *a*, *b*, *c* (Å^2), and eccentricity *e* for GROMOS unrestrained RM systems.

Composition	w_0	I_1	I_2	I_3	*a*	*b*	*c*	*e*
Unrestrained RMs - GROMOS force field								
Eicke	6	3.9 ± 0.7	4.2 ± 0.6	5.4 ± 0.8	23.3 ± 0.3	22.3 ± 0.3	16.3 ± 0.3	0.72 ± 0.02
Waks	6	7.4 ± 0.9	9.2 ± 0.1	11.3 ± 0.2	29.0 ± 0.3	24.6 ± 0.2	18.4 ± 0.2	0.77 ± 0.01
Eicke	10	15.7 ± 0.3	16.8 ± 0.3	22.9 ± 0.5	32.5 ± 0.5	30.9 ± 0.5	20.6 ± 0.5	0.77 ± 0.02
Waks	10	24.2 ± 0.8	31.1 ± 0.9	35.5 ± 0.5	37.4 ± 0.8	30.7 ± 0.7	25.5 ± 0.4	0.73 ± 0.02

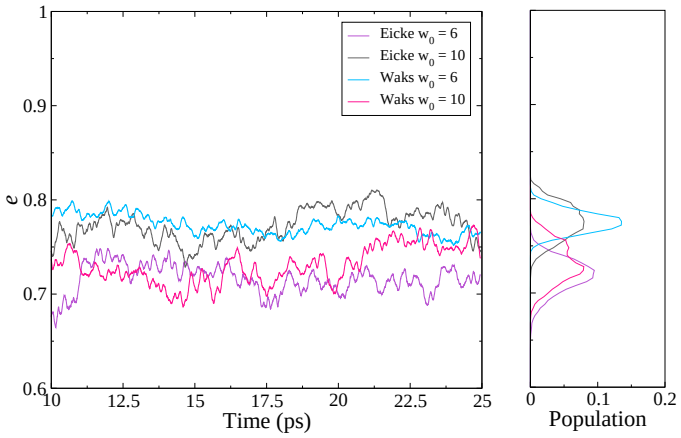

Figure 2: Eccentricity parameter for the GROMOS unrestrained RMs for the last 15 ns of simulation. The eccentricity parameter is plotted versus time (left) with the normalized histogram of eccentricity values shown for the last 15 ns (right).

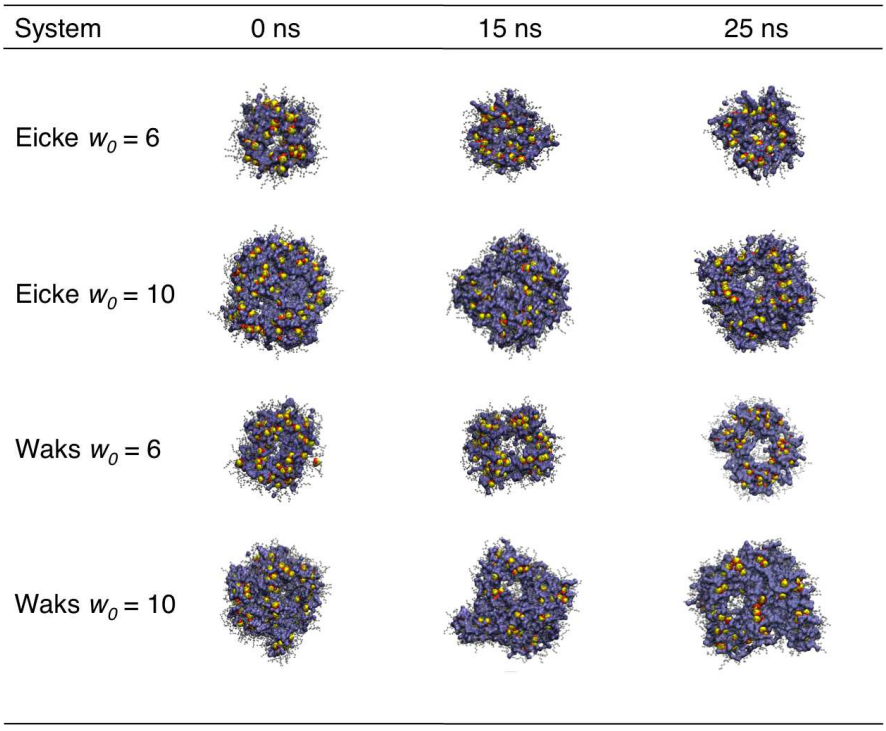

Figure 3: Structures of the unrestrained reverse micelles for the GROMOS force field. The images from left to right show the structures of the RMs at 0, 15, and 25 ns. The AOT sulfur head groups are represented by yellow sulfur atoms and red oxygen atoms. The AOT tails are in gray, and the water is in blue.

Rotional Anisotropy

We extracted decay times from the tri-exponential fits for the first 20 ps of rotational anisotropy decay ACFs (shown in Table 2). The relaxation times of the water in our CHARMM simulations are slower than what Biswas saw, but are in closest agreement with Biswas's surface layer water in RMs of w_0 = 7.5, with one sub-picosecond timescale, one 0.5-1 ps timescale, and one multiple-picosecond timescale.[5] As was the case for Biswas *et al.*[5] and Pieniazek *et al.*,[6] the rotational anisotropy decay times observed for the water in the CHARMM systems are faster than the experimental values for water in RMs of comparable size.[7] They do however follow the experimental trend with the w_0 = 6 RMs having longer decay times than the w_0 = 10 RMs. For the GROMOS systems, while the rotational anisotropy decay times for the SPC water are much longer than for the TIP3P water, the simulations also follow the experimental trend with the water in the w_0 = 6 RMs also showing longer decay times than the water in the w_0 = 10 RMs. For bulk water simulations the rotational anisotropy relaxation time for the TIP3P water model is also faster than for SPC water model: ~2.2 ps compared to ~3 ps.[8]

Table 2: Rotational anisotropy decay times for the first 20 ps of the ACFs fit to:
$\boldsymbol{f(x) = C_0 e^{-x/\tau_0} + C_1 e^{-x/\tau_1} + C_2 e^{-x/\tau_2}}$

Composition	w_0	C_0	τ_0 (ps)	C_1	τ_1(ps)	C_2	τ_2(ps)	error
Unrestrained RMs - CHARMM force field								
Eicke	6	0.44	0.085	0.44	1.43	0.17	12.0	± 0.00329
Waks	6	0.43	0.084	0.43	1.52	0.14	12.5	± 0.00326
Eicke	10	0.41	0.081	0.50	1.12	0.09	8.1	± 0.00224
Waks	10	0.40	0.085	0.49	1.24	0.11	8.7	± 0.00239
Unrestrained RMs - GROMOS force field								
Eicke	6	0.19	0.007	0.09	2.10	0.71	118.5	± 0.00181
Waks	6	0.28	0.069	0.08	2.70	0.72	145.0	± 0.00038
Eicke	10	0.22	0.007	0.18	2.18	0.60	54.2	± 0.00422
Waks	10	0.24	0.082	0.16	2.92	0.59	60.7	± 0.00103
Restrained RMs - CHARMM force field								
Eicke	6	0.36	0.007	0.49	1.08	0.15	9.8	± 0.00958
Waks	6	0.36	0.007	0.49	1.07	0.14	11.0	± 0.01086
Eicke	10	0.32	0.007	0.56	0.93	0.12	7.6	± 0.00744
Waks	10	0.32	0.007	0.56	0.95	0.12	8.4	± 0.00772

We also obtained τ and β values from the stretched exponential fits for the first 10 ps of the rotational anisotropy decay ACFs for the CHARMM systems (shown in Table 3).

Table 3: Rotational anisotropy decay times for the first 10 ps of the ACFs fit to: $f(x) = e^{-(x/\tau)^{\beta}}$

Composition	w_0	τ (ps)	β
Unrestrained RMs - CHARMM force field			
Eicke	6	0.74	0.42
Waks	6	0.61	0.50
Eicke	10	0.85	0.43
Waks	10	0.66	0.47
Restrained RMs - CHARMM force field			
Eicke	6	0.71	0.44
Waks	6	0.69	0.43
Eicke	10	0.63	0.49
Waks	10	0.64	0.49

Water Mobility

Water diffusion rates show strong force field dependence To help explain the difference in rotational anisotropy decay times between the two water models, we calculated the mean square displacement (MSD) and diffusion coefficient for the water in each of the unrestrained RMs for the last 2000 ps of simulation. As the motion of water molecules in the RM is limited to the water pool, the diffusion is bounded and it is not possible to estimate the diffusion coefficient through fits to the asymptotic dependence of the mean-square displacement (at long times). As such, these results we present provide insight in the time scale of water motion but are not intended to represent well-defined diffusion coefficients for the water. For these calculations we used linear fits to the initial mean-square displacement as a function of time. We found that TIP3P in a reverse micelle environment is more mobile and has a higher diffusion coefficient than SPC. Figure 4 shows the MSD for the last 2000 ps of simulation. Table 4 shows the diffusion coefficients calculated for the water in all unrestrained RM systems for the last 2000 ps. Both the MSD and diffusion coefficients indicate that the TIP3P water model is less restrained than the SPC water model in the RMs. While this trend is also seen for bulk water, the difference is not as pronounced with diffusion coefficients having been reported as ~6.0 x 10^{-5} cm^2/s for TIP3P and ~4.3 x 10^{-5} cm^2/s for SPC.[9]

Prior computational studies using SPC have shown the diffusion coefficient for water near a membrane interface to decrease significantly.[10,11] van Hijkoop *et al.* studied the diffusion of water through a membrane protein channel using the SPC water model. The diffusion coefficient they

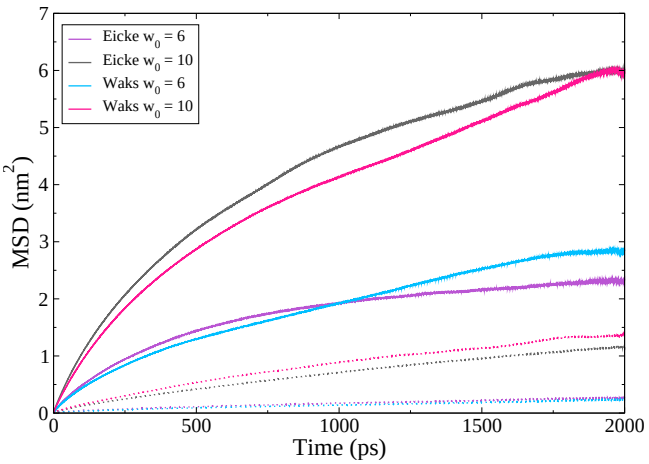

Figure 4: Mean square displacement (MSD) of the water in the unrestrained RMs for the last 2000 ps of the simulations. The solid lines represent the CHARMM systems and the dotted lines represent the GROMOS systems. This plot shows that that TIP3P water model is more mobile than SPC in the RM environment.

report for water molecules trapped by the channel wall is 0.055 x 10^{-5} cm^2/s which is on the same order of magnitude as our SPC water in RMs of $w_0 = 10$.[10] Tieleman and Berendsen studied a similar system using the SPC water model and reported that the diffusion coefficients decreased by almost an order of magnitude as compared to bulk in the narrowest part of the channel.[11]

References

[1] Phillips, J. C., Braun, R., Wang, W., Gumbart, J., Tajkhorshid, E., Villa, E., Chipot, C., Skeel, R. D., Kaleé, L., and Schulten, K. (2005). Scalable Molecular Dynamics with NAMD. *J. Comput. Chem. 26*, 1781–1802.

[2] Oostenbrink, C., Villa, A., Mark, A. E., and van Gunsteren, W. F. (2004). A Biomolecular Force Field Based on the Free Enthalpy of Hydration and Solvation: The GROMOS Force-Field Parameter Sets 53A5 and 53A6. *J. Comput. Chem. 25*, 1656–1676.

[3] Eisenhaber, F., Lijnzaad, P., Argos, P., Sander, C., and Scharf, M. (1995). The Double Cubic Lattice Method: Efficient Approaches to Numerical Intergration of Surface Area and Volume and to Dot Surface Contouring of Molecular Assemblies. *J. Comput. Chem. 16*, 273–284.

Table 4: Diffusion coefficients for water in unrestrained RMs for the last 2000 ps of the trajectories. The diffusion coefficients are higher for the TIP3P water indicating that it is more mobile than the SPC water in the RMs. TIP3P also has a higher diffusion coefficent than SPC in bulk water where the values are reported to be 6.0 x 10^{-5} and 4.3 x 10^{-5} cm^2/s for TIP3P and SPC respectively.[9]

Composition	w_0	Water Model	D (10^{-5} cm^2/s)
Unrestrained RMs - CHARMM force field			
Eicke	6	TIP3P	0.13 ± 0.15
Waks	6	TIP3P	0.21 ± 0.05
Eicke	10	TIP3P	0.40 ± 0.32
Waks	10	TIP3P	0.39 ± 0.19
Unrestrained RMs - GROMOS force field			
Eicke	6	SPC	0.02 ± 0.01
Waks	6	SPC	0.02 ± 0.00
Eicke	10	SPC	0.09 ± 0.03
Waks	10	SPC	0.11 ± 0.04

[4] Eisenberg, D., and McLachlan, A. D. (1986). Solvation Energy in Protein Folding and Binding. *Nature 319*, 199–203.

[5] Biswas, R., Chakraborti, T., Bagchi, B., and Ayappa, K. (2012). Non-Monotonic, Distance Dependent Relaxation of Water in Reverse Micelles: Propagation of Surface Induced Frustration Along Hydrogen Bond Networks. *J. Chem. Phys. 137*, 014515.

[6] Pieniazek, P. A., Lin, Y.-S., Chowdhary, J., Ladanyi, B. M., and Skinner, J. L. (2009). Vibrational Spectroscopy and Dynamics of Water Confined Inside Reverse Micelles. *J. Phys. Chem. B 113*, 15017–15028.

[7] Piletic, I. R., Moilanen, D. E., Spry, D., Levinger, N. E., and Fayer, M. (2006). Testing the Core/Shell Model of Nanoconfined Water in Reverse Micelles Using Linear and Nonlinear IR Spectroscopy. *J. Phys. Chem. A 110*, 4985–4999.

[8] Wu, Y., Tepper, H. L., and Voth, G. A. (2006). Flexible Simple Point-Charge Water Model with Improved Liquid-State Properties. *J. Chem. Phys. 124*, 024503.

[9] Mark, P., and Nilsson, L. (2001). Structure and Dynamics of the TIP3P, SPC, and SPC/E Water Models at 298 K. *J. Phys. Chem. A 105*, 9954–9960.

[10] van Hijkoop, V. J., Dammers, A. J., Malek, K., and Coppens, M.-O. (2007). Water Diffusion Through a Membrane Protein Channel: A First Passage Time Approach. *J. Chem. Phys. 127*, 085101.

[11] Tieleman, D., and Berendsen, H. (1998). A Molecular Dynamics Study of the Pores Formed by Escherichia coli OmpF Porin in a Fully Hydrated Palmitoyloleoylphosphatidylcholine Bilayer. *Biophys. J. 74*, 2786–2801.